Chapter 5

Oxidation of the Pt(111) surface

5.1 Introduction

The oxidation of metal surfaces has been studied for many years using a vast range of surface science techniques due to the wide use of metal oxide surfaces in modern industry [11, 16, 123–127]. Platinum is one of the most important metals used in modern heterogeneous catalytic processes. It is used in the oxidation of CO and the reduction of NO molecules in vehicle exhaust systems, as well as in the oxidation of NH_3 molecules to form nitric acid [128, 129]. Factors affecting the adsorption of O on to Pt surfaces, a vital stage in such processes, include the nature of the oxygen species to which the surface is exposed (molecular or atomic), the oxygen concentration and the temperature of the Pt surface during the adsorption process. Varying such parameters can change both the concentration of O atoms adsorbed on the surface and the strength with which they are bound to the substrate material.

The adsorption of molecular oxygen on the Pt(111) surface has been studied using a wide range of techniques. Early work by Puglia *et al.* identified the formation of four distinctly different adsorption phases [130]. Initially, a physisorbed state is formed when molecular oxygen was adsorbed at a temperature of 25 K. As the temperature increased, two molecular chemisorbed phases were observed at temperatures of 90 K and 135 K. No comments as to the order of the surfaces were made, but all four phases were found to have an oxygen saturation coverage of $\sim$ 0.33 ML or below. Above 150 K, the formation of an atomic chemisorbed state with a p(2×2) LEED pattern was observed, indicative of the dissociation of O_2 on adsorption. Gland *et al.* identified the existence of a molecular species on the surface when at a temperature of less than 150 K, which dissociated to an atomic chemisorbed state with a p(2×2) LEED pattern above 150 K [131]. The atomic chemisorbed state was found to have a saturation coverage of $\sim$ 0.25 ML. These findings have since been confirmed using

a range of techniques including NEXAFS [130], TPD [132] and EELS [133].

Several groups have observed oxygen coverages in excess of the 0.25 ML saturation coverage achievable when using O_2 at relatively low temperatures and pressures. Gland achieved this by external atomisation of the oxygen molecules [134], whilst Steininger *et al.* used electron beam induced dissociation of O_2 molecules which had been adsorbed on the surface [135]. Both groups found that the maximum coverage of adsorbed O could be increased by approximately a factor of two using these methods and found a p(2×2) ordered O adlayer. Interestingly, Steininger *et al.* also observed a $(3\sqrt{2}\times 3\sqrt{2})$R15° reconstructed oxygen adlayer prior to dissociation of the adsorbed O_2 molecules. The molecules were adsorbed at 100 K, so the observation of an ordered adlayer offers new information which was not discussed by Puglia [130].

Using thermal desorption techniques, Segner and co-workers observed an increased O coverage by exposure of the Pt(111) surface to NO_2, producing a coverage of 0.77 ML [136]. This approach yields a surface with little long-range order, as shown by Parker and co-workers [132]. The method relies on the dissociation of NO_2 to NO and O on adsorption to the Pt surface. The NO molecules are then desorbed by annealing to 400 K, leaving the O atoms on the surface. Whilst 400 K is insufficient to desorb the O atoms, the thermal energy input provides enough energy for the O atoms to form a poorly ordered adlayer.

Derry and Ross observed a three to five fold increase in the O coverage by exposure of the Pt(111) surface to higher pressures of O_2 ($\sim 10^5$ mbar) at elevated temperatures (570 K) [133]. Whilst Pt-oxide formation was considered unlikely by these authors, it could not be entirely ruled out. No observation of the order of the system was discussed and therefore it is difficult to speculate further on the location of the O atoms within the structure.

In summary, whilst higher oxygen coverages were achieved by several methods, the groups concerned all concluded that the states formed were chemically identical to the atomic chemisorbed state formed at a coverage of 0.25 ML. No significant penetration of O into the bulk Pt structure, and hence sub-surface oxide formation, was conclusively demonstrated.

Recently Carlisle *et al.* proposed that there is a critical coverage, θ_c^{thd}, at which the transition between the formation of the chemisorbed oxygen phase and the formation of an oxide state occurs on the Ag(111) surface [29]. Furthermore, this transition was said to be thermodynamically, and not kinetically, determined. Below θ_c^{thd}, the heat of adsorption is higher than the heat of formation of the oxide, and hence favours the formation of the chemisorbed phase. As the O coverage increases, the repulsive interactions between the O atoms leads to a decrease in the differential heat of adsorption, until it equals the heat of formation of the oxide at θ_c^{thd}. Hence at coverages in excess of θ_c^{thd}, the formation of an oxide is favoured. This trend has been attributed to the energy required to distort the Pt lattice and initiate the formation of the oxide layer [137]. Initially an oxygen overlayer is chemisorbed on the surface. However, as the O layer becomes more densely packed, the O atoms are driven into more favourable sub-surface sites. Recently, Weaver *et al.* determined the O coverage beyond which oxidation begins on the Pt(111) surface to be $\sim$ 0.75 ML using LEED, XPS and EELS [138].

In this chapter, both a high oxygen concentration state formed on the Pt(111) surface and the p(2×2) reconstruction formed after annealing of the high oxygen concentration state have been investigated using CAICISS, LEED and XPS [139]. Such a combination of techniques allows the study of surface periodicity, structure and composition. The Pt surface was exposed to atomic oxygen, rather than molecular O_2, in an effort to increase the coverage of O atoms adsorbed on the surface and hence exceed θ_c^{thd}. Since atomic O is more reactive than its molecular counterpart, O_2, and with O coverages in excess of 0.25 ML previously obtained using atomic O adsorption, it is possible that θ_c^{thd} may be more readily approached, or even exceeded, using this method of deposition.

5.2 Experimental details

The Pt(111) crystal was cleaned *in-situ* using cycles of IBA (surface bombarded with 3 keV Ar^+ for 30 minutes, followed by annealing at 800°C for 1 hour). Impurities such as Ca and Si have previously been observed to enhance oxidation of the Pt

surface at high temperatures [140, 141]. With this in mind, XPS was used following each IBA cycle to monitor for impurities. The Al K_α anode of the X-ray source was used ($h\nu$ = 1486.6 eV), with all binding energies calibrated relative to the Pt $4f_{7/2}$ peak at 70.9 eV [142]. The analyser was operated in a fixed analyser transmission (FAT) mode with a pass energy of 25 eV. IBA cycles continued until a (1×1) LEED pattern and a contaminant-free XPS spectrum were recorded. Once clean, CAICISS data were recorded from the surface in the $< \bar{2}11 >$ and $< \bar{1}10 >$ azimuths (see figure 5.1). The surface was then exposed to atomic oxygen via the thermal gas cracker, mounted with a direct line-of-sight to the sample surface. Atomic oxygen exposures were carried out at room temperature at pressures of 10^{-7} to 10^{-8} mbar, with the cracker having an estimated 60% cracking efficiency for O_2 [143]. Resistive heating of the sample following oxygen exposure (up to 500°C) was monitored using a chromel-alumel thermocouple in contact with the sample. All CAICISS data were

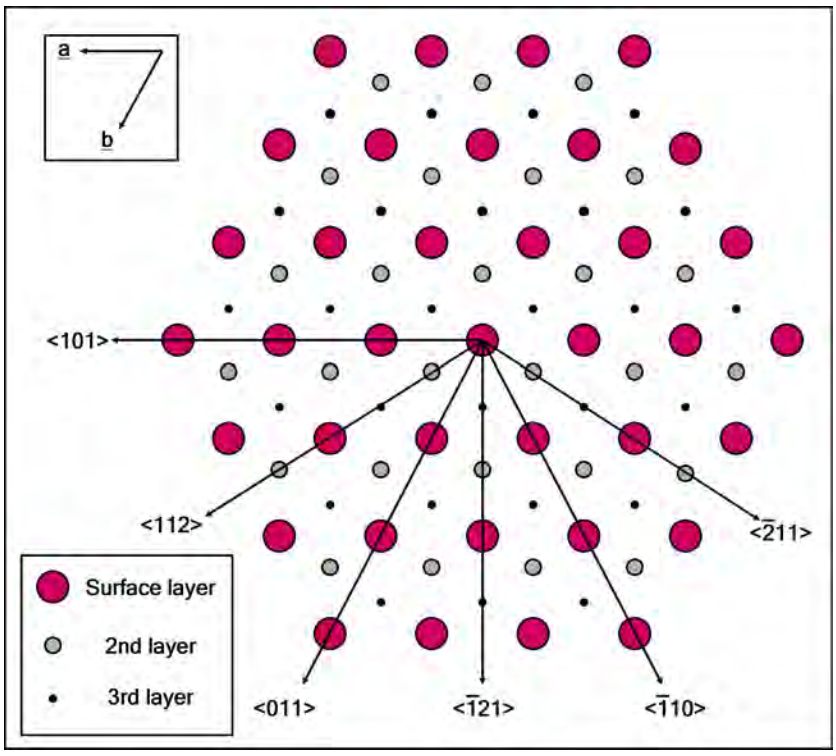

Figure 5.1: The (111) surface of an fcc crystal with some low-index azimuthal directions labelled. CAICISS data were taken from the Pt(111) surface in the $< \bar{2}11 >$ and $< \bar{1}10 >$ azimuths. The inset in the upper-left shows the unit vectors on the fcc (111) surface.

recorded using a 3 keV He^+ ion beam, with spectra collected at 1.8° intervals in the polar angle between 0° and 180°.

5.2.1 Scattering geometries

A plan view of the atomic structure of the three outermost layers of an fcc(111) surface (e.g. Pt(111)) is shown in figure 5.1. Several high symmetry directions exist within the crystal plane which offer the opportunity to probe the structure of the surface region using CAICISS. Figure 5.2 shows cross-sections of the two geometries chosen for the ion scattering experiments presented in this chapter. In the $< \bar{2}11 >$ azimuth, geometries exist where the surface layer atoms focus the incident ions on

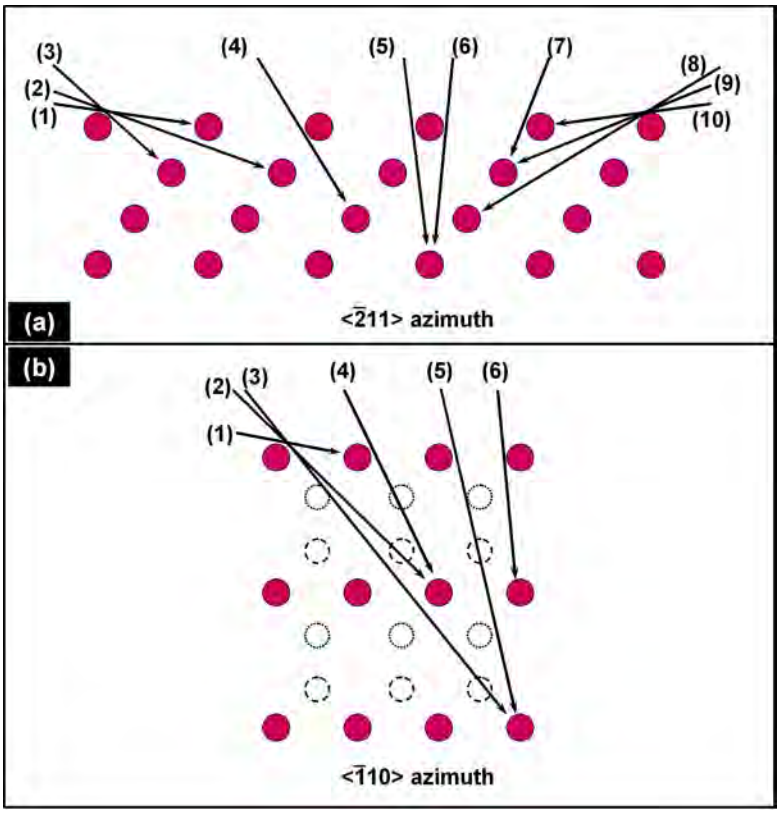

Figure 5.2: The scattering geometries which lead to peaks in CAICISS spectra obtained in (a) the $< \bar{2}11 >$ and (b) the $< \bar{1}10 >$ azimuthal directions on the Pt(111) surface. This combination of azimuthal directions allows a full structural determination down to the seventh layer of the crystal. Atoms represented by dashed lines lie in different planes with respect to the incident ion beam.

to atoms in the surface layer (labelled directions 1 and 10), second layer (directions 2, 3, 7 and 9), third layer (directions 4 and 8) and fourth layer (directions 5 and 6). The $< \overline{1}10 >$ azimuth offers the opportunity to probe more deeply into the Pt(111) structure. Here, scattering geometries exist which give information on the spacing between the first, fourth and seventh layers in the structure (the geometries illustrated in figure 5.2(b)). These geometries also offer information on the distance between the second, fifth and eighth layers as well as the third, sixth and ninth layers. Therefore, any differences between the distance between layers 1 to 4, 2 to 5 and 3 to 6 due to relaxations in the outermost layers will exhibit themselves as shoulders on the peaks at different polar angles in the CAICISS spectra. Therefore, the combination of the $< \overline{2}11 >$ and $< \overline{1}10 >$ azimuths allows a full structural determination of the surface region of the Pt(111) crystal to be constructed.

5.3 Results

5.3.1 CAICISS study of the clean Pt(111) surface

Following the completion of the IBA cleaning procedures outlined above and the observation of a (1×1) LEED pattern (shown later in figure 5.8(a)), CAICISS data were taken from the surface in the $< \overline{2}11 >$ and $< \overline{1}10 >$ azimuths. Figure 5.3 shows a set of ToF spectra (i.e. backscattered intensity as a function of the time-of-flight), taken at polar angle intervals of 1.8° in the $< \overline{2}11 >$ azimuth. A slice was then taken through this plot, integrating the intensities in a ToF range of 5.43 μs to 5.48 μs at each angle, in order to produce a plot of the backscattered intensity as a function of polar angle for all particles elastically backscattered from Pt atoms in the surface region, as shown in figure 5.4(a).

A structural analysis of the data was carried out using the FAN simulation program, the result of which is shown in figure 5.4(b), whilst the derived surface structure is shown in figure 5.5. The spectra presented in figure 5.4 shown several peaks due to different scattering geometries which were analysed using the FAN simulation software. The peaks at polar angles of 13° and 167° correspond to scattering geometries 1 and 10 in figure 5.2. Fitting of these peaks using the FAN simulation package led

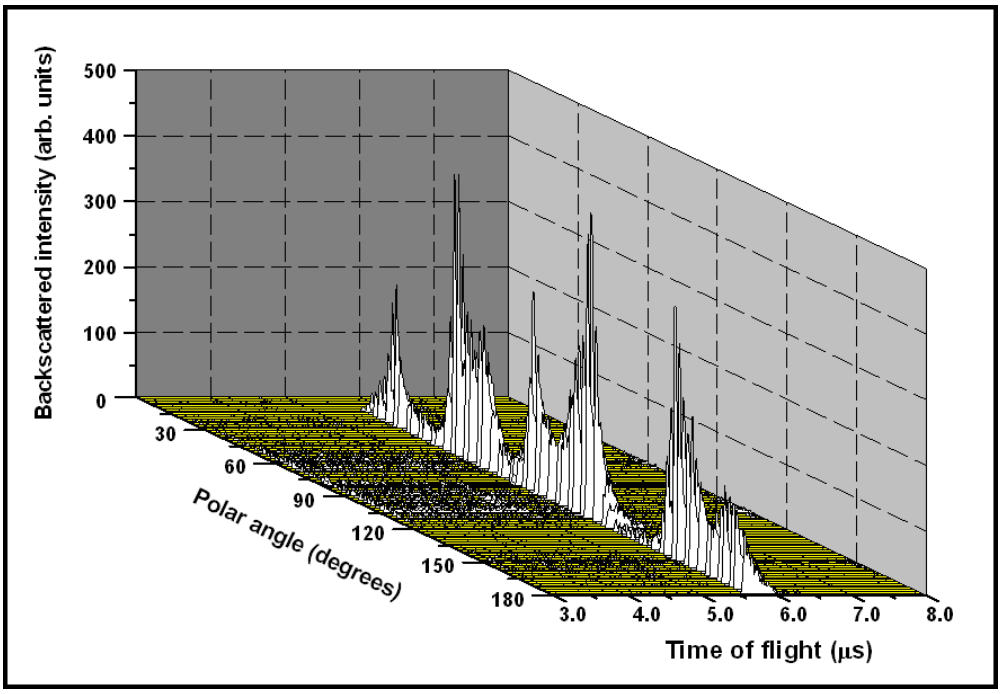

Figure 5.3: The backscattered intensity as a function of time-of-flight (ToF) and energy from the Pt(111) surface. A slice was taken through this plot between flight times of 5.43 μs and 5.48 μs in order to generate the intensity against polar angle plot shown in figure 5.4(a).

to the deduction of the interatomic spacing on the surface in the $< \bar{2}11 >$ direction of 4.81 $\pm$ 0.02 Å. This corresponds to a lattice constant of 3.92 $\pm$ 0.02 Å, corresponding well with previously published values [12, 144]. The peaks observed at 23°, 50°, 107° and 150° correspond to geometries in which the incident beam is focussed on to atoms in the second atomic layer of the structure (directions 2, 3, 7 and 9 in figure 5.4(a)). Fitting of these peaks yielded a first-to-second interlayer spacing, Δ_{12}, of 2.30 Å, corresponding to a 2% expansion relative to the bulk interlayer spacing of 2.26 Å. Similarly, the peaks at 59° and 143° were used to derive the distance between the first and third atomic layers, a value found to be 4.70 Å. Hence, the separation of the second and third layers, Δ_{23}, was found to be 2.40 Å, which corresponds to an expansion of 6% with respect to the bulk interlayer spacing. Finally, the peak at 82° and the shoulder at 98° were used to derive a value for Δ_{34} of 2.26 Å. Therefore, the Pt(111) structure was found to be bulk-like heading deeper into the structure from

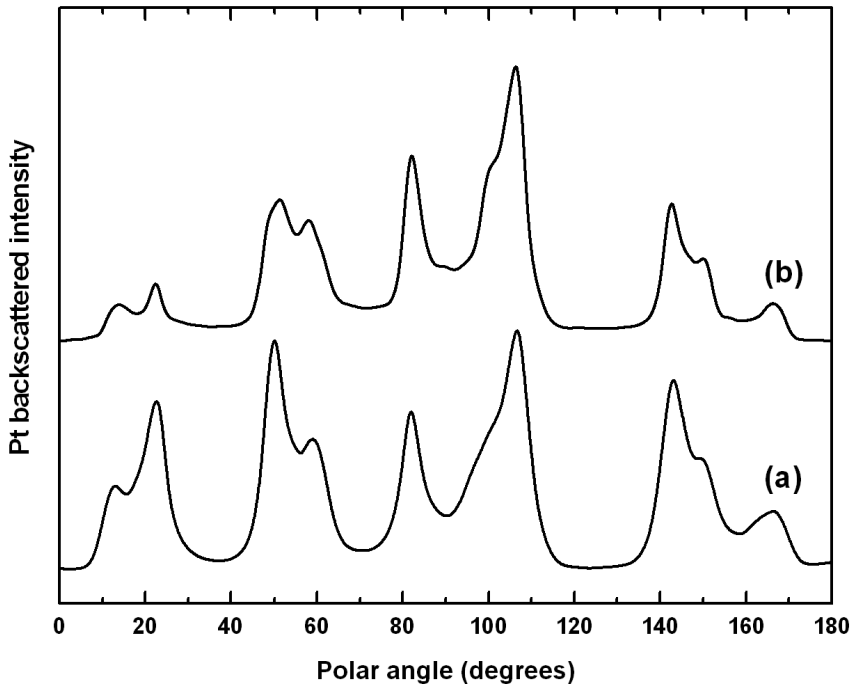

Figure 5.4: (a) Pt backscattered yield as a function of polar angle from the clean Pt(111) surface in the $< \bar{2}11 >$ azimuth. (b) shows a simulation of the trial structure (detailed in the main text and figure 5.5) in the same azimuth.

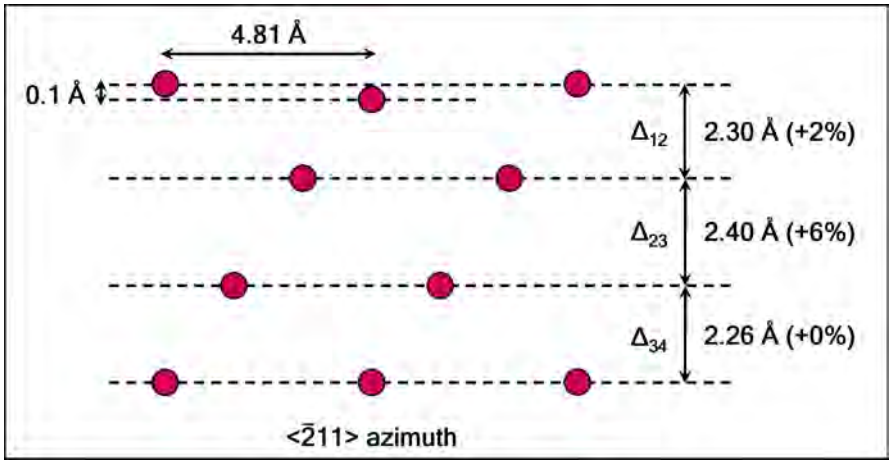

Figure 5.5: The structure of the clean Pt(111) surface derived from analysis of the CAICISS data presented in this chapter. Shown here is a cross-section of the structure, as seen in the $< \bar{2}11 >$ azimuth, with relaxations present in the outermost three atomic layers of the crystal. Data recorded in the $< \bar{1}10 >$ direction showed evidence for a rumpling of 0.1 Å in the surface layer.

the third atomic layer. All interlayer spacings given above are accurate to $\pm$ 0.02 Å.

It should be noted that some slight disagreement in the backscattered intensities between the experimental and simulated spectra exists. This may be due to a small fluctuation in the current delivered to the surface during the course of the 26 hour experiment or a very low amount of contamination which migrated to the surface during the experiment (ie. sufficient to focus a proportion of the incident ions on to atoms within the Pt(111) structure, but insufficient to change the LEED pattern observed). Alternatively, this could be due to the experimental data being recorded in 1.8° polar angle intervals, whereas the simulation progresses in 1.0° intervals.

A similar methodology was used in the analysis of the CAICISS data recorded in the $< \bar{1}10 >$ direction, shown in figure 5.6, with the structure shown in figure 5.5 derived from analysis of these experimental data in conjunction with the data in the $< \bar{2}11 >$ direction presented above. In the $< \bar{1}10 >$ case, only a 90° polar scan was necessary as the atomic structure is symmetric about the surface normal in this

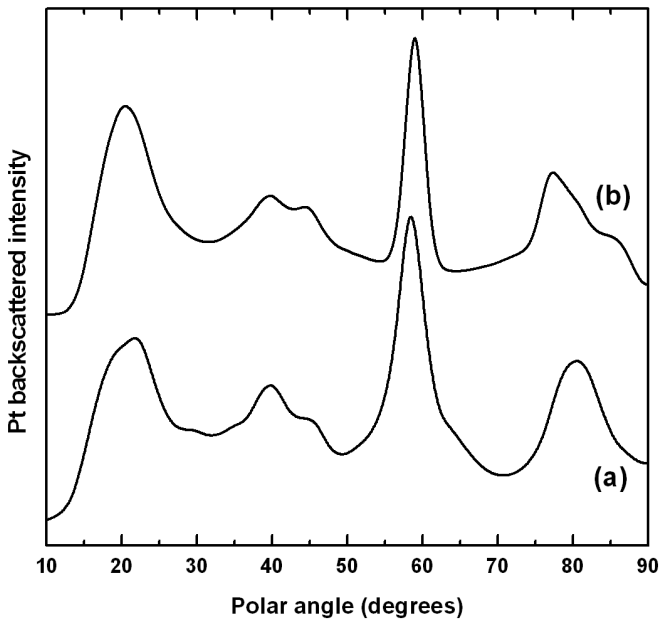

Figure 5.6: (a) Pt backscattered yield as a function of polar angle from the clean Pt(111) surface in the $< \bar{1}10 >$ azimuth. (b) shows the simulated Pt-backscattered profile in the same azimuthal direction, using the structure shown in figure 5.5.

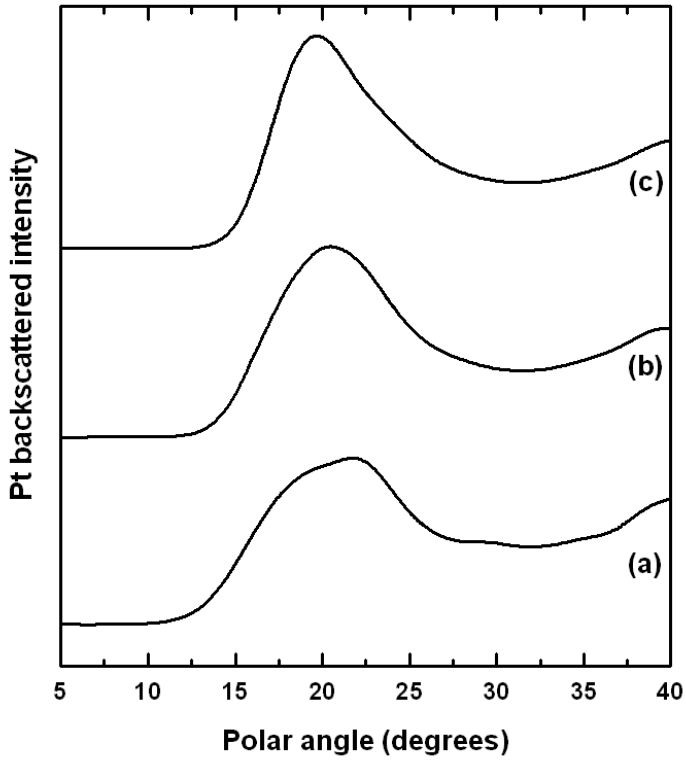

Figure 5.7: (a) Pt backscattered yield as a function of polar angle from the clean Pt(111) surface in the $< \bar{1}10 >$ azimuth. Also shown are the corresponding trial structure simulations, (b) including 0.1 Å surface rumpling and (c) a flat surface layer. The broader surface peak, with an additional component centered at approximately 22°, is only observed in the simulated spectra upon the inclusion of a rumpled surface.

particular azimuth, as shown in figure 5.2(b). The feature at 21° corresponds to the surface critical angle, with analysis of this feature using FAN again leading to the deduction of a lattice constant of 3.92 ± 0.02 Å. However, the peak is rather broad, indicating that it comprises two separate components. Further analysis of this peak, shown in figure 5.7, reveals the existence of a 0.10 ± 0.02 Å rumpling in the surface layer. Neighbouring Pt atoms in the surface layer were found to be out-of-plane by ∼ 0.1 Å. This small difference between the scattering geometries of neighbouring atoms is sufficient enough to give rise to a surface peak with the two components observed in the CAICISS data. The features at 40°, 45° and 58° in figure 5.6 correspond to scattering geometries 2 to 4 in figure 5.4(b), with the feature at 80° containing information from scattering geometries 5 and 6. The broadness of the peaks indicates

some degree of surface relaxation with Δ_{14}, Δ_{25} and Δ_{36} having different values. Analysis revealed Δ_{14} to be 6.96 $\pm$ 0.02 Å, 2% expansion on the bulk value of 6.78 Å. This total expansion of 0.18 $\pm$ 0.02 Å corresponds well with the total expansion in the three outermost layers derived from the data recorded in the $< \overline{2}11 >$ azimuth.

In summary, the clean Pt(111) surface simply corresponds to a truncation of the bulk structure, with some small changes to the interlayer spacings and a small degree of rumpling ($\sim$ 0.10 Å) on the surface. The relaxations observed are in line with previous studies of the Pt(111) surface [12,145,146]. However, the observed rumpling of the surface has not previously been reported. Due to the high surface specificity of the CAICISS technique, this type of feature can be readily observed. Whilst the degree of surface rumpling is only small (4% of the bulk interlayer spacing), it is sufficient to speculate that stresses which may exist in the surface region were reduced by the formation of a rumpled surface.

5.3.2 LEED study of atomic oxygen adsorption on to Pt(111)

A LEED investigation was carried out to monitor the changes to the structure and periodicity of the Pt(111) surface on exposure to atomic oxygen (O*) at room temperature. Figure 5.8 shows the progression of the observed LEED patterns as a function of oxygen exposure. Initially, a p(2×2) pattern was observed after a 5 L O* exposure. The relatively low background intensity and sharpness of the pattern (figure 5.8(b)) indicated a reasonably well-ordered oxygen overlayer. Such a pattern has previously been shown to correspond to oxygen adsorbed in three-fold fcc hollow sites [147, 148].

Following a total O* exposure of 10 L, the background of the p(2×2) pattern was observed to have increased (figure 5.8(c)). This may be an indication of disorder in the O adlayer, or of disruption to the structure of the Pt lattice in the surface region due to O adsorption. Upon reaching an exposure of 20 L, the p(2×2) features were completely obscured by the increased background intensity (figure 5.8(d)). In addition, streaks emanating from the integral order spots were observed. Such features have also been observed by Saliba *et al.* whilst studying oxygen adsorption on the Au(111)

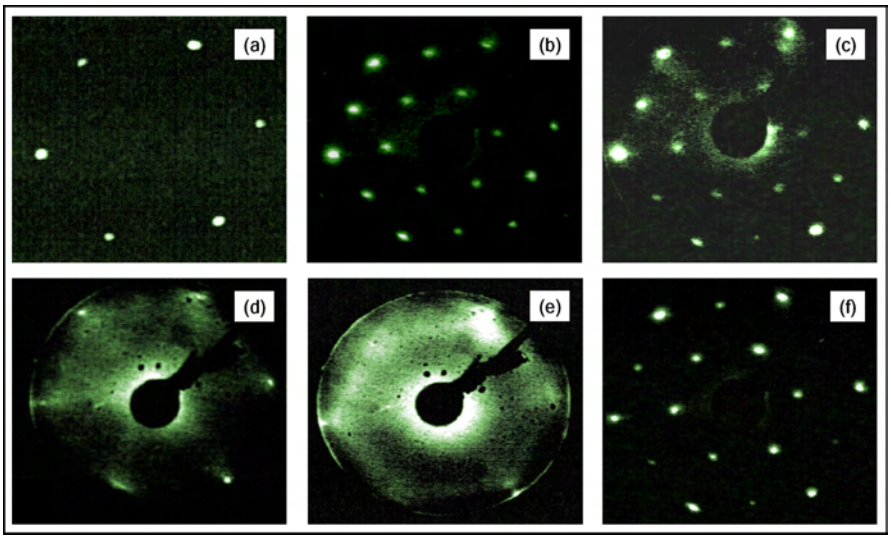

Figure 5.8: LEED patterns, all recorded at an incident electron energy of 84 eV, observed during the exposure of the Pt(111) surface to atomic oxygen. Image (a) shows the (1×1) reconstruction observed from the clean Pt(111) surface. p(2×2) patterns were also recorded after O* exposures of 5 L (b) and 10 L (c), whilst the background intensity obscured the LEED spots after exposures of 20 L (d) and 50 L (e). The p(2×2) pattern shown in image (f) was taken following annealing at 500°C for 20 minutes, discussed further in section 5.3.4.

surface [149], and were attributed to one-dimensional ordering of the oxygen adlayer. It is therefore reasonable to speculate that a similar process could occur on the Pt(111) surface. Atomic oxygen exposure continued up to a total exposure of 50 L (figure 5.8(e)), at which point the substrate integral order spots were completely obscured by the background intensity. These observations are in close agreement to those of Weaver *et al.* who observed the formation of a Pt-oxide beyond an O coverage of $\sim$ 0.75 ML [138].

It should be noted that throughout these studies, care was taken to minimize the time during which the surface was exposed to the electron beam. Electron-stimulated desorption of chemisorbed atoms from metal surfaces is a well known phenomenon [150, 151]. This desorption process cannot be due to direct momentum transfers from the incident electron to the adsorbed atom. Such a transfer imparts only $\sim$ 0.5 eV of kinetic energy on to the adsorbed atom, which is insufficient to overcome the bond strength between a chemisorbed atom and the substrate ($\sim$ 1-10 eV). Instead, ESD arises from a variety of electronic energy transfer mechanisms

between the incident electron and the desorbed atom and are discussed in detail elsewhere [150, 151]. Even at electron energies in the region of 100 eV, significant electron stimulated desorption of O from the surface was observed to occur over a beam exposure period of approximately 10 minutes. Hence, care was taken to minimise these effects by limiting the time taken to record each image to $\sim$ 30 s.

5.3.3 The high O concentration state

5.3.3.1 Chemical nature of the surface region

Following the exposure of Pt(111) to 50 L of atomic oxygen, CAICISS and XPS were used to investigate the structural and and chemical properties of the surface. Of particular interest were the sites at which the O atoms reside and to what extent the Pt surface had been oxidised.

A clear indication of oxide formation was observed in the Pt $4f$ photoemission peak. Analysis of the spectrum, shown in figure 5.9, shows the existence of four

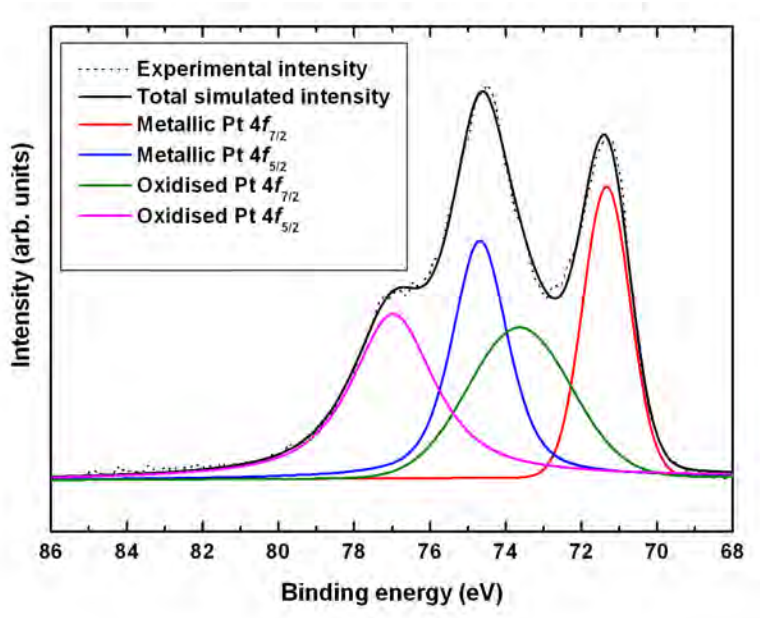

Figure 5.9: The Pt $4f$ region recorded from the O-saturated surface. Four components were required to fit the spectrum, corresponding to metallic Pt $4f_{7/2}$ (71.2 eV), oxidised Pt $4f_{7/2}$ (73.5 eV), metallic Pt $4f_{5/2}$ (74.5 eV), and oxidised Pt $4f_{5/2}$ (76.8 eV).

separate components. The clean Pt $4f_{5/2}$ and $4f_{7/2}$ features were observed at 74.5 eV and 71.2 eV respectively [142]. However, to fit the spectrum, additional components were required at 76.8 and 73.5 eV, a positive 2.3 eV shift from the peaks observed from the clean Pt(111) surface. Positive chemical shifts of this order have previously been observed for various Pt-oxide states (a summary is shown in table 5.1 [139]), and following the adsorption of O on to various different substrates [152–154]. Hence, for the purpose of this investigation, the components at 76.8 and 73.5 eV in the Pt 4*f* region have been assigned to Pt atoms contained within a Pt-oxide layer.

The O 1*s* photoemission peak obtained from the O-saturated surface is shown in figure 5.10. The peak at 530.5 eV was observed to be slightly asymmetric, with an additional component at a higher binding energy required to fit the overall peak shape. The existence of such a component is also suggested by the broadness of the O 1*s* peak (FWHM of 2.3 eV). The peak profile was modelled using a Gaussian-Lorentzian mixture (70:30), and shows that the overall O 1*s* peak consists of two components.

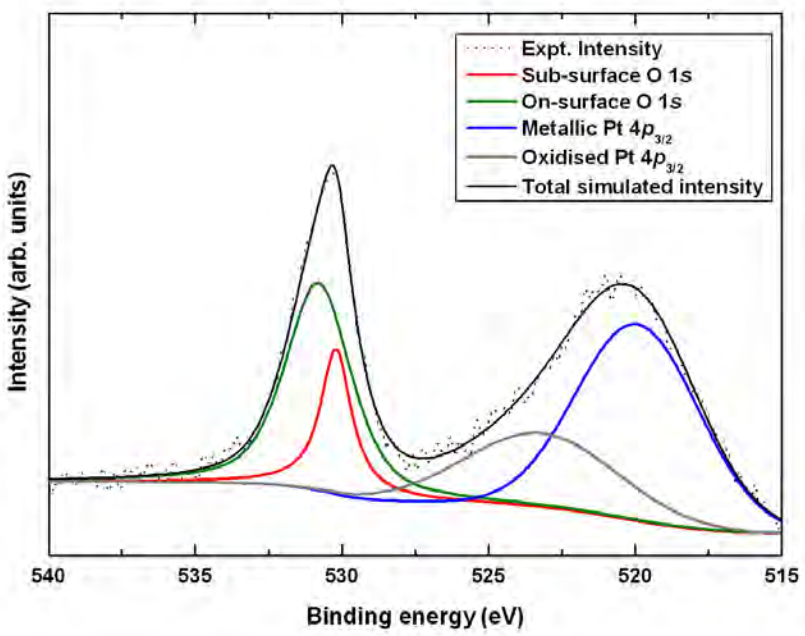

Figure 5.10: The O 1*s* and Pt $4p_{3/2}$ region of the XPS spectrum taken from the saturated Pt surface (50 L O* exposure). Four separate components are required to accurately fit the spectrum, corresponding to on-surface O atoms (530.8 eV), sub-surface O atoms (530.2 eV), Pt atoms in an oxide layer (523.5 eV) and metallic Pt (520.0 eV).

The first, at a binding energy of 530.8 eV, corresponds to chemisorbed oxygen atoms on the surface. The second, at 530.2 eV, corresponds to sub-surface oxygen atoms in a PtO_2 layer [155]. Additional justification of these assignments, from both CAICISS and further XPS data following the annealing, will be given later in this chapter.

With the initial XPS data indicating the existence of oxygen atoms within the Pt substrate, attention was turned to the depth into which the O atoms penetrated. Figure 5.11 shows a series of XPS spectra recorded from the O-saturated surface at a range of take-off angles. Inspection of the spectra revealed a large enhancement of the

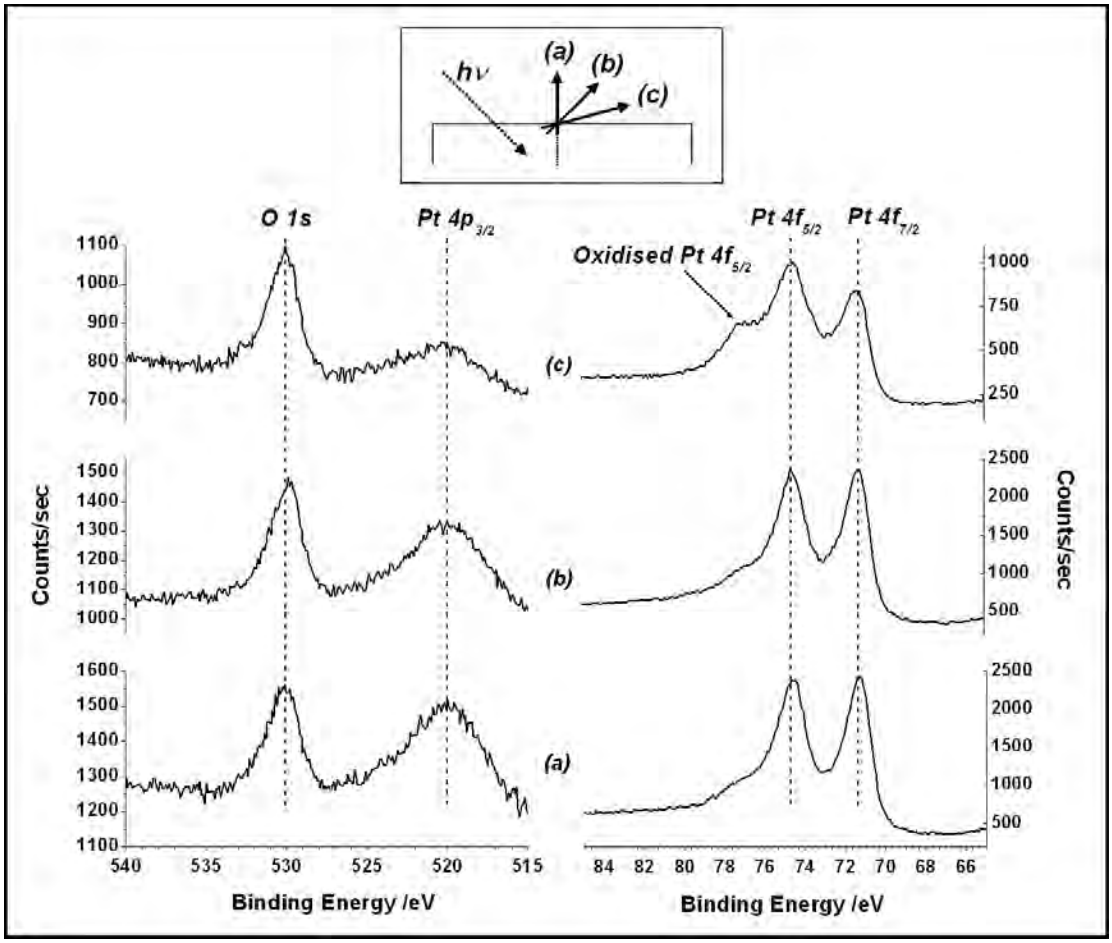

Figure 5.11: XPS data taken following the exposure of a clean Pt(111) surface to 50 L of atomic oxygen. The spectra shown were taken at take-off angles of (a) 90°, (b) 45° and (c) 15°. The inset in the upper part of the figure shows these geometries in more detail, with each geometry obtained by rotation of the sample with respect to the X-ray source and the hemispherical analyser. The angle between the source and the analyser remained at 45° throughout.

O 1*s* peak and the oxide components of the Pt 4*f* spectrum at a take-off angle (TOA) of 15° (the most surface-specific case studied here), suggesting that only a small degree of penetration of O atoms into the Pt bulk structure had occurred. However, the fact that the oxidised Pt component had been observed at all demonstrates that there is indeed some penetration of O into the sub-surface region, leading to the formation of a PtO_2 layer. Therefore the critical coverage, θ_c^{thd}, must have been exceeded by exposing the Pt(111) surface to atomic rather than molecular oxygen.

	Pt 4f$_{7/2}$ (eV)	**Pt 4f$_{5/2}$ (eV)**	**O 1s (eV)**	**Reference**
Pure Pt	71.2	74.5	-	[142]
$Pt_{polycrystalline}$ -O	71.1	74.5	531.6, 530.0	[140]
Pt(111)-p(2×2)-O	70.9	-	529.8	[130]
	71.2	74.5	530.2	[155]
	71.2	74.5	530.8	This work
PtO	72.3	-	530.5	[156]
$PtO_{2(bulk)}$	74.1	77.4	530.1	[155]
PtO_2 on Pt	71.2	74.5	530.2	[155]
High O-conc. Pt	73.5	76.8	530.2	This work

Table 5.1: Example of the Pt 4$f_{7/2}$, Pt 4$f_{5/2}$ and O 1*s* binding energies for clean Pt and Pt-oxide surfaces.

5.3.3.2 Atomic structure of the surface region

To further investigate the penetration depth of the O atoms into the sub-surface region, as indicated by the XPS data presented in the previous section, a CAICISS study was performed in the $< \overline{2}11 >$ azimuth on the O-saturated surface. In a similar fashion to the LEED studies, the time for which the O-covered surface was exposed to the ion beam had to be minimised. Figure 5.12 shows full polar angle CAICISS scans along the $< \overline{2}11 >$ direction from the clean Pt(111) surface, the O-saturated surface and the p(2×2)-O surface (discussed later). These data clearly show the convergence of the profiles from both O-covered surfaces on to that of the clean Pt(111) surface for polar angles greater than 70° (ion beam exposure times in excess of $\sim$ 1 hour). In the case of the O-saturated Pt(111) surface, the existence of a substitutional Pt-oxide would be expected to reveal additional features at around 27°, 50°, 107° and

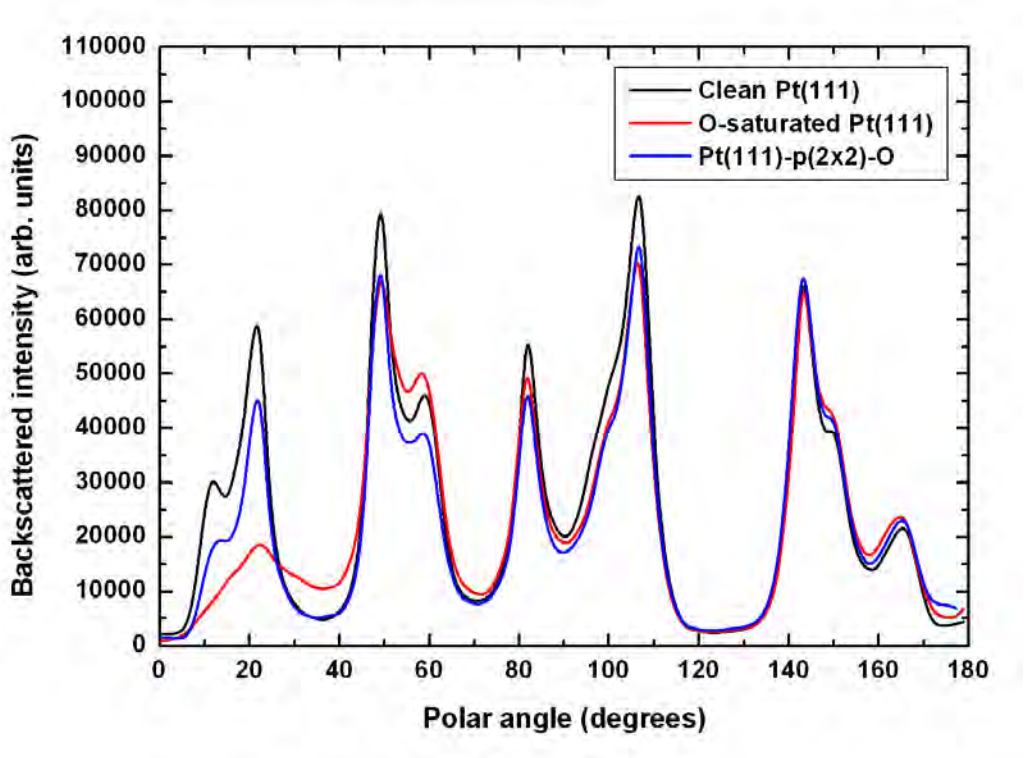

Figure 5.12: CAICISS plots showing the backscattered intensity profile from the clean Pt(111) surface, as well as the effects of ion-stimulated desorption of O atoms from the saturated and p(2×2)-O surface formed on annealing. The full polar scan is shown in each case, with both O-covered surface data sets converging on to the clean Pt(111) data for angles above $\sim 70^{\circ}$.

150° due to the removal of second layer Pt atoms during the formation of the oxide layer. However, the spectrum obtained from the O-saturated surface closely matches that of the clean Pt(111) surface at polar angles in excess of $\sim 70^{\circ}$, indicating that the O atoms in the surface region had been removed as a result of interactions with the incident ions, with the surface reverting back to the clean Pt(111) structure. Subsequent XPS data also suggests the removal of O atoms from the surface due to exposure to the ion beam (a process known as ion-stimulated desorption (ISD)). This process can occur due to the transfer of energy during the collision of the oxygen atom and the incident helium ion being larger than the binding energy of the oxygen atom to the Pt(111) surface [157, 158], or due to charge exchange processes which occur during the scattering process [1]. It has been shown that O atoms desorb from

a variety of surfaces under exposure to a He^+ ion beam in the energy range used in CAICISS, including Pt [157,158], Ni [159] and a number of other surfaces [1,160–164].

In an effort to minimise the effects of the ISD process on the CAICISS data, the rotation axis of the sample was slightly misaligned so that the incident beam spot moved across the sample during the experiment. Experiments were also limited to the first 70° from grazing incidence, with a step duration of 100 s and a 1.8° step interval. With these safeguards in place, no significant degradation of the O concentration was observed, as shown in figure 5.13, which shows distinctly different spectra recorded from the clean Pt(111), O-saturated and p(2×2)-O surfaces. With evidence of only limited O penetration from the XPS data, as well as the significant role played by the ISD process, the implication was that the vast majority of the O atoms were at or near the surface. In the $< \bar{2}11 >$ azimuth, all scattering geometries corresponding

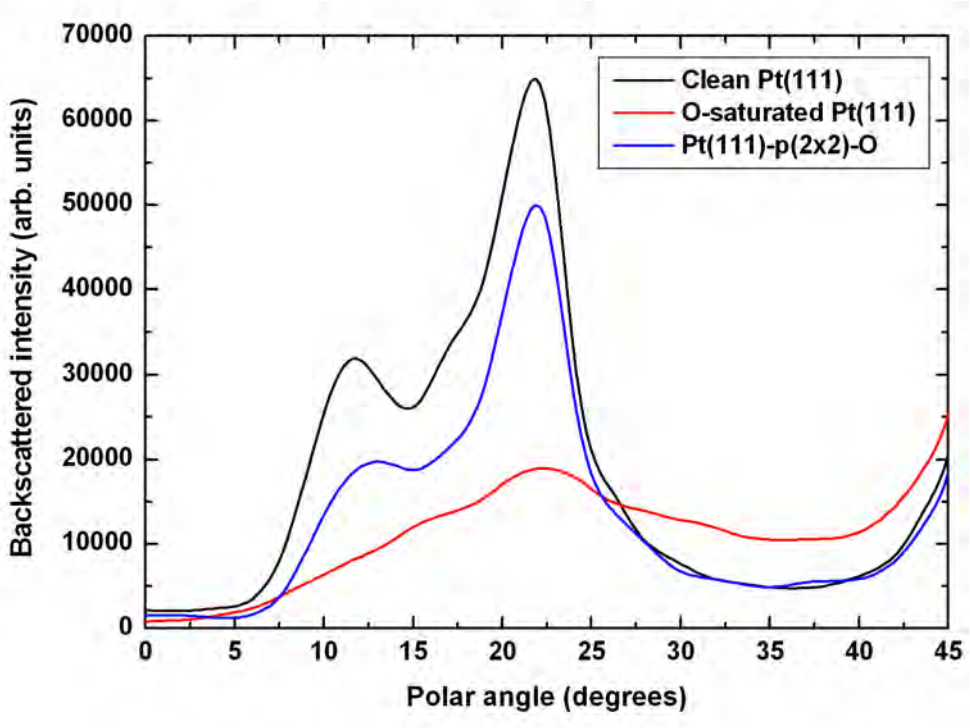

Figure 5.13: The region of interest (ie. the surface peak) from the CAICISS data recorded from the clean, O-saturated and p(2×2)-O Pt(111) surfaces. In this angular range ISD has a limited effect on the surface due to the shortened time of exposure of the surface to the incident ion beam. Clear differences in the Pt-backscattered intensity from the three surfaces were observed in this region.

to scattering from the first, second and third layers are contained within the first 70° of the polar angle scan. Hence it was not necessary to record CAICISS data at polar angles greater than 70°, minimising the probability of the ISD process removing significant quantities of O from the surface region.

With the possibility of ISD affecting the data recognised, CAICISS data were taken in the $< \bar{2}11 >$ azimuth, with the polar angle data acquisition window limited from 0° to 70° (figure 5.14). Comparing the Pt profile with that of the clean surface (shown in figure 5.13), one can immediately see the broadening and the reduction in the intensity of the features within the first 40° of the data collected from the O-saturated surface. This is most likely due to a disruption of the surface structure during the oxidation process caused by the larger lattice parameter of the PtO_2 layer compared to the bulk Pt(111) structure [11]. Such disruption can produce a range of interatomic spacings in the surface layer and hence yield a broadened surface peak.

Figure 5.14 shows simulated Pt backscattered intensities for the two most likely sub-surface O atom sites, both accompanied by the adsorption of O atoms into three-fold hollow sites on the surface, as required to observe the peak at 530.2 eV in the O 1*s* XPS spectrum. Firstly, an interstitial oxide was simulated. In this structure the O atoms occupy the octahedral sites between the first and second layers of Pt atoms. Simulation of this structure, shown in figure 5.14(c), gave rise to no additional peaks in the Pt-backscattered CAICISS spectrum relative to the clean surface. Secondly, a structure was simulated where the adsorbed O atoms form a substitutional oxide by replacing Pt atoms in the second layer. Such a structure allows additional peaks to be observed in the CAICISS spectrum, such as the peak shown at $\sim$ 27° in figure 5.14(b). Such features arise from scattering geometries which would have previously been blocked due to the shadowing effects of a Pt atom in the second atomic layer. However, a proportion of the atoms in the second layer have been displaced during the formation of the oxide layer, allowing atoms from deeper layers to contribute to the backscattered intensity. With reference to figures 5.2(a) and 5.14, the removal of some of the Pt atoms in the second atomic layer leads to the reduction in the intensity of the peak observed at 22° relative to the clean surface (geometry 2 in figure 5.2).

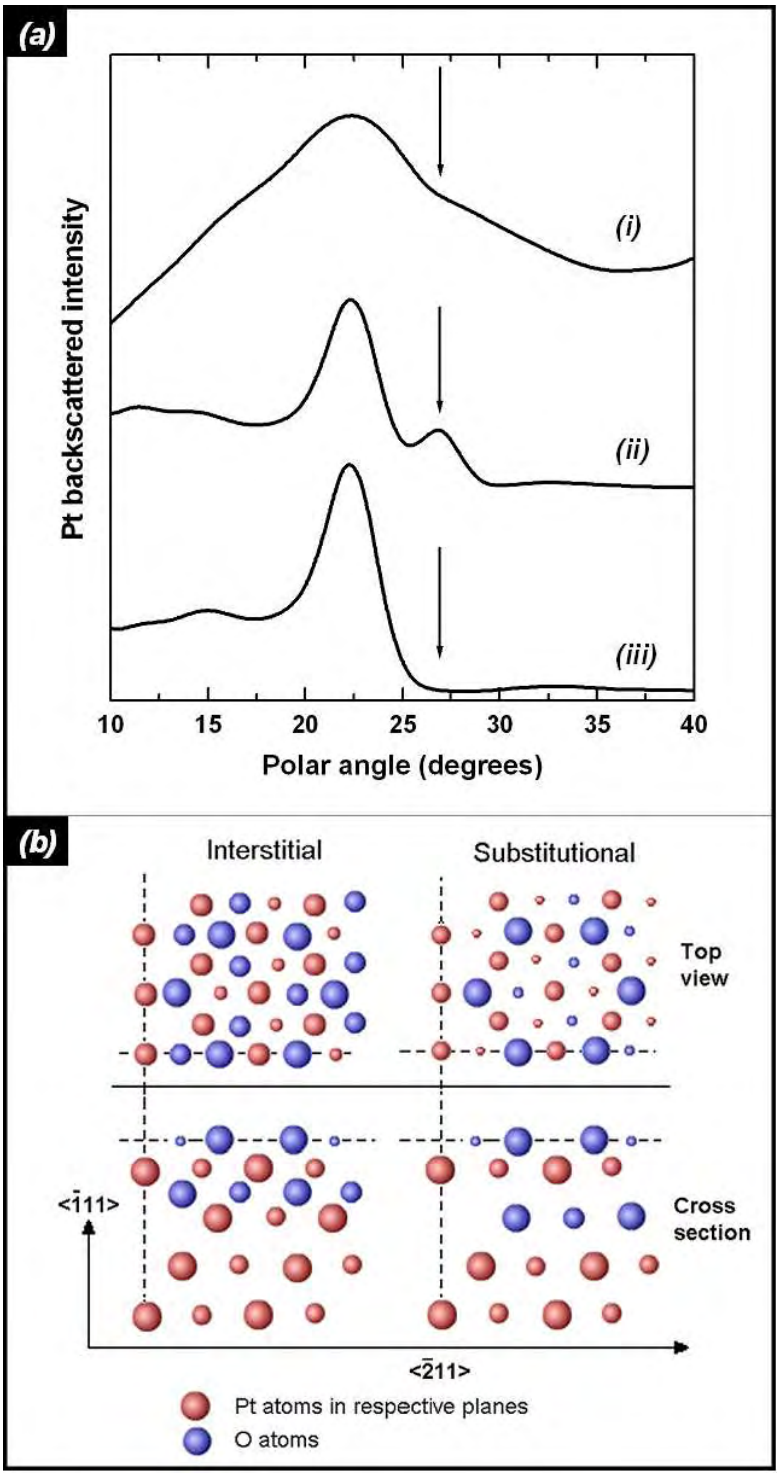

Figure 5.14: (a) (i) CAICISS data from the O-saturated Pt(111) surface, along with simulated profiles for both the (ii) substitutional and (iii) interstitial Pt-oxide structures. The feature observed at 27° in the experimental data is only reproduced by the substitutional Pt-oxide model. (b) The two trial structures (interstitial and substitutional) used to generate the simulated spectra in (a).

The smaller scattering cross-section of the O atoms located in such sites in the Pt-oxide film allows the incident ions to penetrate deeper, striking Pt atoms in the third atomic layer and thus giving rise to the peak observed at 27° in figure 5.14(b).

Figure 5.14(a) shows the experimental profile from the O-saturated Pt(111) surface. This profile contains a suggestion of a feature at 27° corresponding to the formation of a substitutional Pt-oxide layer. However, due to the broadness of this feature and the inability to detect ions backscattered from O atoms, it is not possible to state conclusively that the sub-surface Pt atoms are contained exclusively within a substitutional oxide structure. Such broadness in the experimental profile, most likely due to the formation of a disordered surface, corresponds well with the loss of p(2×2) spots in the LEED pattern observed from the surface (figure 5.8(f)).

Analysis of both the CAICISS data obtained in the first 70° of the polar angle range and the XPS data described above suggested an oxygen saturation coverage of approximately 1.3 ML, well in excess of the 0.25 ML coverage obtained by other groups following the exposure of the Pt(111) surface to O_2. Both techniques indicate the formation of a sub-surface PtO_2 layer at this oxygen coverage, suggesting that the critical coverage for oxide formation can be exceeded by exposing the Pt(111) surface to atomic oxygen.

5.3.4 Formation of the Pt(111) p(2×2)-O surface

The final part of this investigation was focussed on the changes to the composition and structure of the surface after annealing the O-saturated surface. The sharp p(2×2) LEED pattern observed following annealing of the O-saturated surface to 500°C for 20 minutes (figure 5.8(f)), suggests a re-ordering of the oxygen adlayer on the Pt(111) surface with a final coverage in the region of 0.25 ML.

The O 1*s* and Pt 4*f* photoemission peaks recorded before and after annealing are shown in figure 5.15. In the O 1*s* spectrum, the component at 530.2 eV corresponding to oxide formation was observed to be significantly reduced upon annealing with respect to the feature corresponding to O atoms on the surface at 530.8 eV. In addition, the shoulder on the Pt $4f_{5/2}$ peak at 76.8 eV was completely removed by annealing.

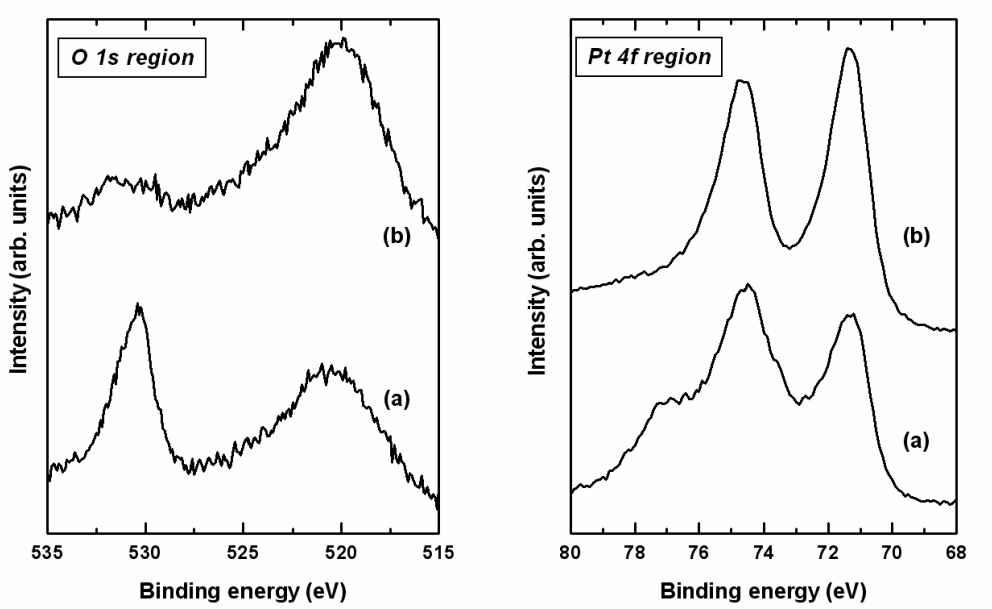

Figure 5.15: Comparison of O 1*s* and Pt 4*f* XPS regions taken from (a) the O-saturated Pt(111) surface and (b) the p(2×2)-O surface formed after annealing at 500°C for 20 minutes. The spectra show the elimination of the peaks corresponding to the sub-surface Pt-oxide (at 530.2 eV in the O 1*s* region and 76.8 eV in the Pt 4*f* region).

Indeed, the component at 530.8 eV has also been significantly reduced in intensity, suggesting that O atoms are desorbed during the annealing process. These changes suggest the elimination of the sub-surface oxide, leaving only adsorbed O atoms on the surface in a p(2×2) reconstruction, with the oxygen coverage decreasing from $\sim$ 1.3 ML to 0.25 ML during the annealing process.

Using CAICISS, it was possible to determine the location of the O atoms on the surface following the annealing treatment. Although the O atoms possess a small differential scattering cross-section and cannot be observed directly, shadowing by the O atoms in the two different sites leads to features at different polar angles in the Pt-backscattered intensity profile. The Pt profile from the p(2×2) reconstructed surface is shown in figure 5.16, along with simulated profiles containing on-surface O atoms in fcc and hcp sites. Two features are highlighted, both suggesting that the O atoms reside in hcp sites on the surface. The feature at 19° in the experimental data clearly

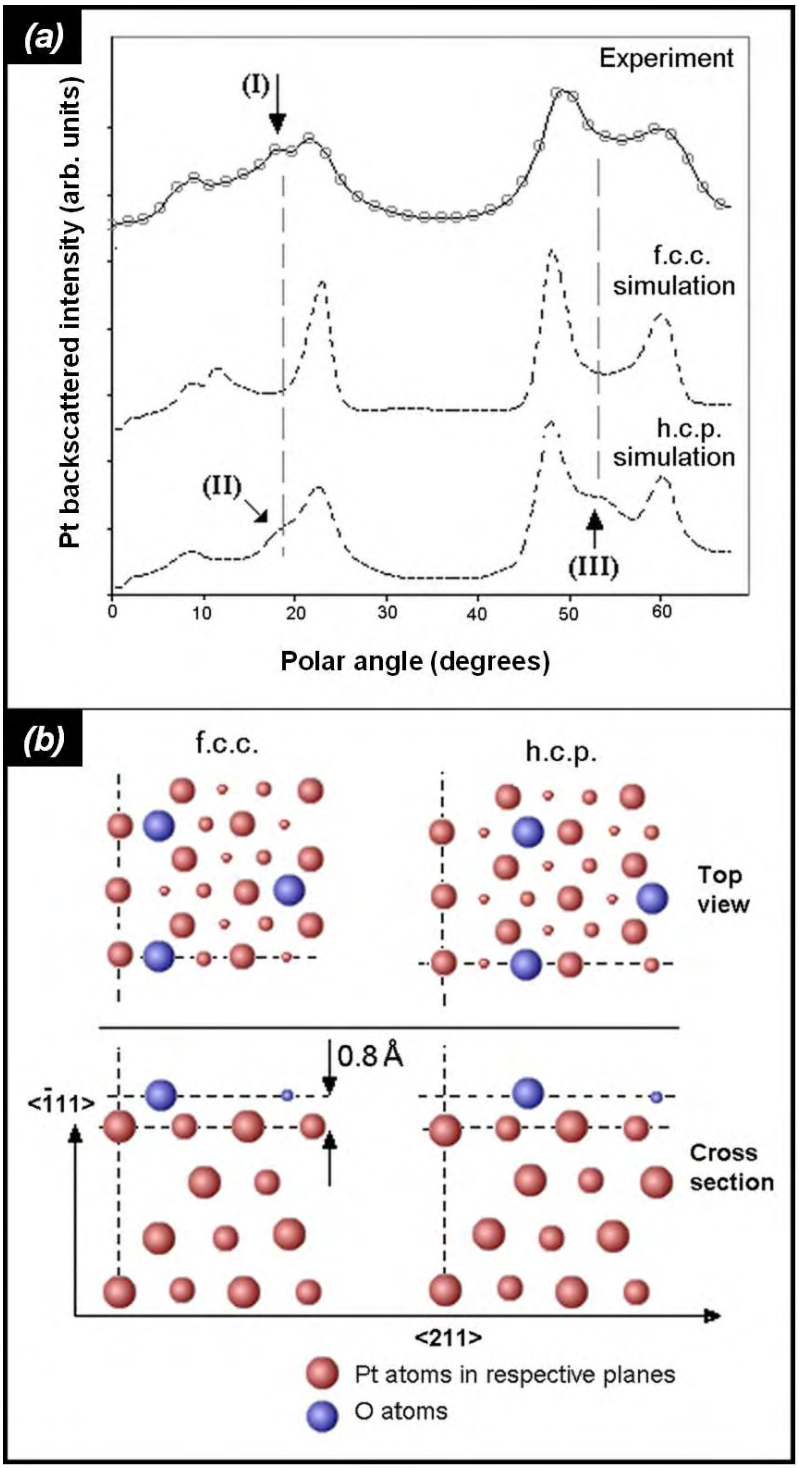

Figure 5.16: (a) CAICISS data from the p(2×2)-O reconstruction formed by annealing the O-saturated Pt(111) surface to 500°C. Also shown are the simulated spectra corresponding to O atoms occupying fcc and hcp sites on the surface. The features at 19° and 53° are observed in both the experimental data and the simulation of O atoms in hcp sites. (b) Schematics of the fcc and hcp structures used to generate the simulated profiles.

indicates that the O atoms reside in the hcp sites. The feature at 53° is less clear, but the increased intensity in this region of the experimental data when compared to the fcc simulation indicates that a small peak, as seen in the hcp simulation, is required to fully replicate the simulated spectrum. The clarity of this feature was potentially hindered by ion-stimulated desorption of O atoms from the surface.

In previous studies it has been shown that the O atoms occupy fcc sites when the p(2×2)-O surface is prepared by exposing the clean Pt(111) surface to oxygen [148]. This is in contrast to the occupancy of hcp sites observed in this investigation following annealing of the oxygen-saturated surface. A similar shift from fcc to hcp sites has also been reported from DFT calculations of O on the Ru(111) surface [165]. Here, the shift was attributed to the slight lowering of the O 1*s* binding energy in the hcp sites relative to the fcc configuration. It is therefore not unreasonable to expect similar behaviour on other transition metal surfaces, and possibly responsible for the observed behaviour on the Pt(111) surface. However, due to the relatively low signal to noise ratio in the O 1*s* XPS spectrum recorded following annealing (figure 5.15), it is not possible to state conclusively that such a shift in the binding energy occurred during annealing.

5.4 Conclusions

In this chapter, the characteristics of the adsorption of atomic oxygen on the Pt(111) surface have been studied using CAICISS, LEED and XPS. It has been demonstrated that a saturation oxygen coverage of greater than 0.25 ML can be obtained by external thermal cracking of the O_2 molecules. The atomic species is highly reactive, allowing the oxygen coverage to exceed the transition point between the kinetic and thermodynamic determination of the formation of either the chemisorbed or oxide phases.

CAICISS data obtained from the clean Pt(111) surface in the $< \bar{2}11 >$ azimuth shows a surface region with small relaxations relative to the bulk structure. The first two interlayer spacings were found to have expanded by approximately 2% and 6% respectively, and are in general agreement with previous studies. In addition, a small

degree of previously unobserved rumpling of the surface was observed, with data in the $< \bar{1}10 >$ azimuth suggesting that nearest neighbours were out of plane by 0.1 Å.

The initial exposure of the surface to 5 L of atomic oxygen led to the formation of a p(2×2) reconstruction. This has previously been shown to be indicative of the formation of an O adlayer on the surface, with O atoms residing in fcc three-fold hollow sites. Further exposure to atomic oxygen led to the masking of the p(2×2) spots by the increasing background intensity. At the saturation O exposure (50 L), only diffuse streaks emanating from the integer order spots were visible above the high background intensity. XPS spectra of the O-saturated surface showed the existence of both on-surface and sub-surface O atoms, suggesting the formation of a sub-surface oxide. Highly surface specific XPS data (recorded at a take-off angle of 15°) showed only limited penetration of O into the Pt(111) structure. CAICISS studies of the O-saturated surface demonstrated the existence of a substitutional oxide in the second layer, in addition to O atoms at the surface in fcc three-fold hollow sites. The broadness of the features in the CAICISS spectrum also indicated substantial surface disorder. This is in agreement with the observed LEED pattern, which exhibited a high background intensity which masked any diffraction pattern. Both CAICISS and XPS data estimated the saturation coverage to be $\sim$ 1.3 ML, well in excess of both the 0.25 ML observed using O_2 and the critical oxygen coverage required for oxide formation.

Annealing of the O-saturated surface to 500°C led to the formation of a p(2×2) surface reconstruction. XPS data showed the removal of the sub-surface oxide species and the existence of O atoms on the Pt surface in the form of an overlayer. CAICISS experiments following annealing showed the surface O atoms to be residing in hcp sites, as opposed to fcc sites when the p(2×2) reconstruction was formed directly following a 5 L exposure. This is attributed to the hcp sites being energetically more favourable relative to their fcc counterparts, as seen in the Ru(111) case [165].

The effects of ESD and ISD have also been demonstrated for the O-covered Pt(111) surfaces, something that should be born in mind for any investigation of chemisorbed species using energetic incident particles. Oxygen atoms were observed

to desorb from the surface after $\sim$ 10 minutes when exposed to an electron beam (E $\sim$ 100 eV) and after approximately 1 hour when exposed to a He^+ ion beam ($E_0 =$ 3 keV).

It has also been shown that the critical coverage for oxide formation on the Pt(111) surface can be exceeded by exposure of the surface to atomic oxygen. The location of O atoms within the structure can be controlled using such an approach, with adsorbed atoms located in fcc sites upon initial adsorption at low O* exposures, before being driven into sub-surface substitutional sites with increasing O coverage. The O atoms can then be relocated into hcp sites on the surface by annealing the Pt-oxide layer to 500°C for 20 minutes.